OMAE-18-1028

Author 1 (Lead author): Lin Li

Mailing address: Department of Mechanical and Structural Engineering and Materials Science, University of Stavanger, Stavanger, Norway
Email: lin.li@uis.no

Author 2 (Corresponding author): Zhiyu Jiang

Mailing address: Department of Engineering Sciences, University of Agder, 4879 Grimstad, Norway

Email: zhiyu.jiang@uia.no

Author 3: Jungao Wang

Mailing address: Norwegian Public Roads Administration, Bergelandsgata 30, 4012 Stavanger, Norway

Email: jungao.wang@vegvesen.no

Author 4: Muk Chen Ong

Mailing address: Department of Mechanical and Structural Engineering and Materials Science, University of Stavanger, Stavanger, Norway
Email: muk.c.ong@uis.no

Numerical study on the heading misalignment and current velocity reduction of a vessel-shaped offshore fish farm

Lin Li[1], Zhiyu Jiang [*2, 3], Jungao Wang[1] and Muk Chen Ong[1]

[1]Department of Mechanical and Structural Engineering and Materials Science, University of Stavanger, Stavanger, Norway

[2]Department of Engineering Sciences, University of Agder, 4879 Grimstad, Norway

[3]Department of Marine Technology, Norwegian University of Science and Technology, Trondheim, Norway

Abstract

Recently, the concept of a vessel-shaped fish farm was proposed for open sea applications. The fish farm comprises a vessel-shaped floater, five fish cages, and a single-point mooring system. Such a system weathervanes, and this feature increases the spread area of fish waste. Still, the downstream cages may experience decreased exchange of water flow when the vessel heading is aligned with the current direction, and fish welfare may be jeopardized. To ameliorate the flow conditions, a dynamic positioning (DP) system may be required, and its power consumption should relate to the heading misalignment. This paper proposes an integrated method for predicting the heading misalignment between the vessel-shaped fish farm and the currents under combined waves and currents. A numerical model is first established for the fish farm system with flexible nets. Current reduction factors are included to address the reduction in flow velocity between net panels. The vessel heading is obtained by finding the equilibrium condition of the whole system under each combined wave and current condition. Then, the Kriging metamodel is applied to capture the relation between the misalignment angle and environmental variables, and the probability distribution of this misalignment angle is estimated for a reference site. Finally, the requirement for the DP system to improve the flow condition in the fish cages is discussed.

[*] Corresponding author. Email address: zhiyu.jiang@uia.no

INTRODUCTION

Many benefits attract the installation of fish farms in exposed seas, including ample space for expansion, tremendous carrying capacity of sea water, reduced conflict with many user groups, lower exposure to human sources of pollution and the potential to reduce negative environmental impacts. However, significant technical and operational challenges exist due to harsh environmental conditions. Fish farming in fully exposed offshore areas requires new engineering approach since equipment and methods currently used in protected nearshore areas are mostly unsuitable for open seas [1]. Therefore, it is essential to develop novel and robust offshore fish farms to meet the challenges.

The Norwegian aquaculture industry has recently proposed several new and potential fish farm concepts for open seas. By the end of 2017, five concepts had been granted development licenses from the Directorate of Fisheries in Norway. The five concepts include two closed concepts, one semi-closed concept and two open cage offshore fish farms. One open cage design, the semi-submersible fish farm 'Ocean Farm 1' developed by Ocean Farming AS, is the world's largest fish farm to be installed in exposed offshore areas [2]. This design combines technology from both the aquaculture industry and the offshore oil and gas industry. The pilot facility has been installed at an exposed coastal site of central Norway in 2017 [3]. Norway Royal Salmon AS and Aker Solutions ASA proposed another semi-submersible fish farm, and the global response analysis of a similar structure under waves has been carried out in both frequency and time domains [4].

Another open cage fish farm is the vessel-shaped fish farm named 'Havfarm' proposed by Nordlaks AS; see Figure 1. Several cages are distributed along the longitudinal direction of the vessel. Two different 'Havfarm' concepts were suggested using different positioning systems: the stationary and the dynamic farms. The stationary farm is positioned using a passive single point mooring system connected at the bow of the vessel. Thus, the heading of the whole farm will be determined by the wind, wave and current loads and their directions. The dynamic farm, on the other hand, will not have a permanent mooring system, but mainly rely on the dynamic positioning (DP) and propulsion systems to maintain its position and to relocate. The energy consumption as well as the operational and maintenance cost may increase substantially compared to the stationary farm.

This paper addresses numerical study of a vessel-shaped fish farm, which is modified based on the design of the stationary 'Havfarm' as shown in Figure 1. Global response analysis of this structure in combined currents and waves has been presented in our previous publications [6, 7]. The whole fish

Figure 1: Overview of the vessel-shaped fish farm concept [5].

farm is a weathervaning unit and allows the structure to head to the currents and waves under most conditions. In such situations, the downstream cages may experience reduced water exchange compared to the upstream cages due to the shielding effects since the whole farm consists of several cages in a row with small distances in between.

In reality, the water flow in and around the open fish cages is complex and affected by several factors, including the physical properties of the cage structure [8], bathymetry [9], farm organization [9] and the movement of the fish themselves [10]. Extensive investigations, both numerically and experimentally, have been carried out in recent decades to understand the flow fields of a net cage, examples can be found in [11, 12]. Although the local flow conditions around the nets are complex and three-dimensional, these studies generally revealed that water motion helps to maintain the water quality in a net cage and sufficient water exchange is important for the health and growth of the fish.

From operational point of view, to improve the water exchange, one good solution is to rotate the whole structure to be misaligned with the current direction. So, the shielding effects from the upstream cages can be mitigated. To realize this, in practice, a DP system with thrusters may be needed to counteract the environmental loads and to change the heading of the structure. Because of the high energy consumption, it is important to estimate the power required of the DP system in the design phase. The DP power requirement can be predicted once the minimum required current velocity in the cages is known. For the vessel-shaped fish farm, due to the shielding effects from the upstream nets, the current velocity depends strongly on the misalignment angle between the heading of the vessel and the currents.

Thus, the focus of this study is to investigate the misalignment angle of the whole fish farm and current velocity reductions in the fish cages under realistic environmental conditions. The purpose is to provide useful information for design of the DP system to improve the flow condition in the fish cages. A numerical

model of the coupled fish farm system, including the vessel, the flexible fish cages and the single-point mooring system is firstly established. Then, an integrated method using Kriging metamodels is proposed and applied for the calculation of the misalignment angle for a reference site. Irregular deep-water waves and uniform currents are assumed in the analysis. The probability distribution of the misalignment angle for this site is predicted. By using a simple estimation of the current reduction factor inside each cage, the current velocities inside the cages are obtained. Finally, the requirement for using the DP system to improve the water exchange is discussed.

DESCRIPTION OF THE VESSEL-SHAPED FISH FARM

The whole fish farm consists of a vessel-shaped floater, five flexible fish cages, and a mooring system. In our study, we used a simplified floater design compared to 'Havfarm' to simplify the analysis. The floater consists of a bow, two main longitudinal support beams, and transverse beams to strength the main support beams. In normal operational conditions, only the bow and the longitudinal beams are submerged. This provides a large opening area for the cages. Steel louse skirts are designed to isolate the fish from the currents in the upper layer to reduce possible influences of sea lice [5].

The main set-up of the concept and the dimension of the submerged part of the vessel is illustrated in Figure 2. The structure has a total length of 400 m, a breadth of 50 m and a draft of 10 m. Five cone-shaped cages are connected to the floater at 10 m below the mean water surface. At this draft level, the minimum horizontal gap between two neighboring cages is 10 m. Each cage has a 48-m diameter at the top and a depth of 50 m. A bottom weight of 4 tonnes is hanging under each cage to tension the net and maintain the volume of the cage. The material properties of the fish nets are shown in Table 1. The solidity ratio of the nets is defined as the ratio of the projected area of the bars and knots of the nets to the total outline area of a netting panel. The common netting materials have solidity ratios in the range of 0.2 to 0.3 [13]. In the numerical analysis, two solidity ratios of 0.2 and 0.3 are chosen for comparative studies.

Table 1: Properties of the fish nets

Solidity ratio	[-]	0.2, 0.3
Twine thickness	[m]	0.005
Density	$[kg/m^3]$	1120
Elastic modulus	[MPa]	900

A single-point mooring system is proposed consisting of six mooring lines with 60 degrees spacing

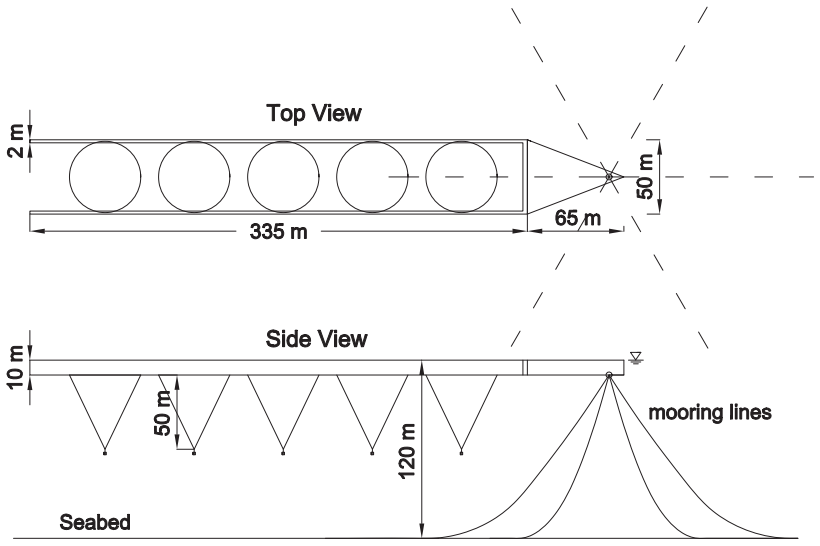

Figure 2: Main geometry of the submerged part of the vessel-shaped fish farm.

in between. The mooring lines are connected to the turret located at the bow; see Figure 2. Such a configuration allows the vessel to weathervane passively with minimal stress on the mooring system. Under extreme environmental conditions, the turret can be efficiently disconnected from the vessel, making it possible for the whole fish farm to move to a sheltered area.

Each mooring line is composed of four segments, including a chain segment, a wire rope segment, and two links between the segments and the fairlead. The chain segments provide adequate restoring forces when the horizontal displacements of the turret are large. The length of the wire ropes should be adequent to avoid possible contact with the seabed under mean drift and dynamic responses. The geometry of the mooring lines does not interfere with the cone-shaped fish cages during motion. Detailed properties of the mooring line components are listed in Ref. [7]. The total length of each mooring line needs to be adjusted based on the water depth of the selected site.

NUMERICAL MODEL

The coupled numerical model of the fish farm, including the floater, the flexible nets and the single-point mooring system, has been established using SIMA (SIMO and Riflex) program developed by SINTEF Ocean [14, 15, 16]. SIMO models the rigid body hydrodynamics of the floater structure and Riflex models flexible elements for the fish nets and the mooring lines using finite element methods. Figure 3 presents the top view of the coupled numerical model. The global coordinate system (with origin at the turret center), definition of the wave and current directions, and the cage and mooring line numbers are also

shown. The modeling considerations as well as the theoretical background are briefly discussed as follows.

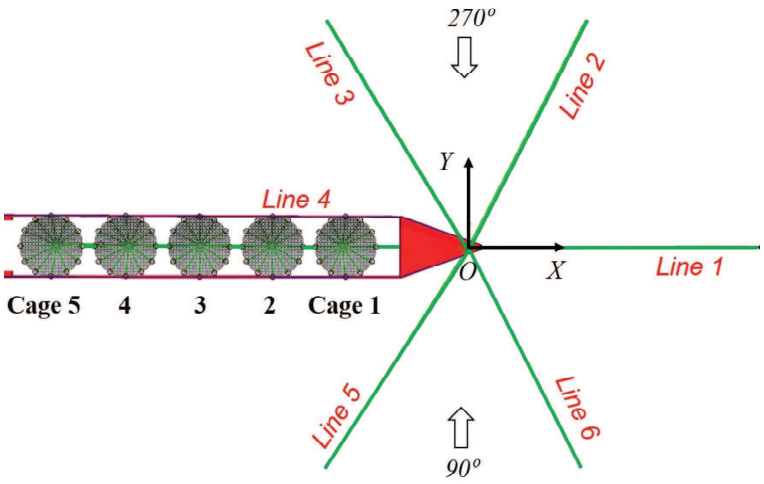

Figure 3: Illustration of the coupled fish farm model with global coordinate system and mooring line numbers

Hydrodynamics of the floater

The hydrodynamic properties of this vessel-shaped fish farm concept were obtained in the frequency domain. A first-order panel model was generated in the Wadam program [17]. Linear potential theory was applied across relevant wave frequencies (from 0.16 to 1.6 rad/s) for all six degrees of freedom of the rigid body motions. Ref. [6] presented the added mass, damping and response amplitude operators (RAOs) of the fish farm for various models with and without rigid net elements. It was shown that the addition of the nets contributes significant viscous damping to the rigid body motions of the floater. The RAOs of the floater were greatly reduced when including the nets, in particular with a higher solidity ratio.

In this paper, the mean drift wave forces on the floater are used in the calculation of the static equilibrium of the whole structure under waves and currents. Moreover, additional viscous damping in terms of Morison elements have been added to the support beams and the bow of the floater. The support beams are rectangular thin plates, and the nondimensional drag coefficient in the beam sea direction was chosen as 2.3 for the relevant Reynolds number range ($\mathrm{Re} > 10^5$) [18]. The viscous damping on the triangular shaped bow was modeled using three beams on the edges of the triangular. Equivalent drag coefficients on the beams in vertical and horizontal directions were selected based on the two-dimensional coefficients from DNV recommended practice [19].

Modeling of flexible nets

The fish nets are flexible structures, and the cages will experience different degrees of deformation depending on the wave and current conditions. The drag and lift forces of the net elements changes with the deformation. In the numerical model, each cage is divided into 12 net panels circumferentially. Each net panel is then represented by a slender line consisting of bar elements, as shown in Figure 4. Equivalent properties of the twines within the net panel are calculated based on the input using Table 1 and applied to the bar elements, including mass, volume and axial stiffness. The drag (F_D) and lift (F_L) forces on a net panel are calculated as:

$$F_D = \frac{1}{2}\rho C_D A \cdot U_{rel} \cdot |U_{rel}| \tag{1}$$

$$F_L = \frac{1}{2}\rho C_L A \cdot U_{rel} \cdot |U_{rel}| \tag{2}$$

where ρ is the water density, A is the area of the net panel, U_{rel} is the relative flow velocity, including current and wave induced fluid velocities. In the present model, the hydrodynamic drag and lift coefficients of the net panel, C_D, C_L are empirical coefficients based on model test data [20].

$$C_D = 0.04 + (-0.04 + 0.33S_n + 6.54{S_n}^2 - 4.88{S_n}^3)cos\theta \tag{3}$$

$$C_L = (-0.05S_n + 2.3{S_n}^2 - 1.76{S_n}^3)sin2\theta \tag{4}$$

where S_n is the solidity ratio of the net panel. The angle of attack, θ, is defined as the angle between the flow direction and the normal vector to the net panel in the direction of the flow. Under different environmental conditions, θ of each bar element will change due to deformation of the net panels, and the total drag and lift forces will change accordingly. The above empirical values are limited to S_n ranging from 0.13 to 0.32 [21].

Current velocity reduction factor

Due to the loss of momentum when water flows through a net panel, a continuing reduction of flow velocity occurs in the downstream cages. This is especially important for the present concept where several net

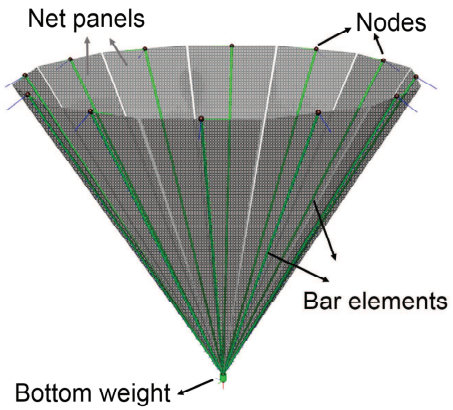

Figure 4: The flexible fish net model using representative bar elements.

cages are positioned in a row. Here we define the current reduction factor, R as follows:

$$R = 1 - \frac{u_i}{U_\infty} \tag{5}$$

where U_∞ is the incoming current velocity. u_i is the local current velocity felt by the i^{th} net panel facing the flow. In reality, the flow around the net structures is complex and three dimensional. The flow may be partly redirected due to the resistance of the nets, biofouling and motion of the fish [8]. All these factors will influence the local current velocity, u_i, and its direction. However, in this study we assume uniform flows before and after passing the net panels and apply the simple engineering approach suggested by Løland [20] for calculation of the local velocities on the net panels.

$$u_i = U_\infty \cdot (1 - R) = U_\infty \cdot (1 - r)^{i-1} \tag{6}$$

$$r = 0.46 \cdot C_D \tag{7}$$

where r is the current velocity reduction factor behind one net panel. C_D is the drag coefficient on the net panel, and it depends on the solidity ratio S_n; see Eq. (3). For a given S_n ($S_n = 0.2$ in our case) with the corresponding C_D, the local current velocity, u_i at each net panel only depends on the value of i. The value $(i-1)$ indicates how many times of reduction the net panel experiences. The requirement of using the above equations is that the distance between the net panels is large enough for the wake to be fully developed, i.e. about 50-100 times the twine diameter. This requirement is satisfied for the studied model. For the vessel-shaped fish farm consisting of five fish cages, different net panels on the same cage may experience different current reductions, depending on the position of the net panels and the relative

current directions. The calculation of the i values for different conditions are illustrated in Figure 5.

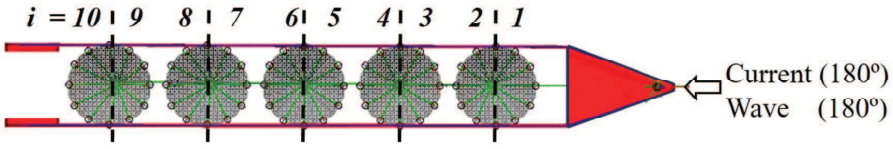

(a) Vessel aligned with the currents

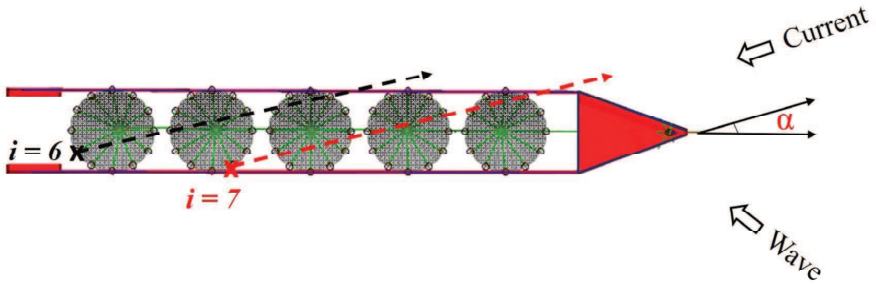

(b) Vessel misaligned with the currents

Figure 5: Illustration of the calculation of i values in Eq. (6) for reduced current velocity under two conditions.

When the currents and waves are aligned, see Figure 5(a), the vessel will position itself heading to the currents (both current and wave directions are 180 degrees). Because each cage consists of front and rear parts, i from 1 to 10 are used for corresponding net panels from Cages 1 to 5.

Under misaligned conditions, there will be a certain misalignment angle, α, between the heading of the vessel and the current direction in the equilibrium position, as shown in Figure 5(b). The local current velocity at the net panels along one cage will be different, depending on the shielding effects from the nets in the upstream. The following method is proposed to find the i values for calculation of the current velocity reduction. First, an artificial line is drawn from each net panel (modeled as slender line with bar elements) parallel and opposite to the current coming direction. Second, the intersections of the line are found with the other cages in the upstream of the net panel. Each intersection accounts for one count of shielding. Finally, the i-value corresponds to the total number of intersection. Two examples are given with i values equal to 6 and 7 respectively in Figure 5(b).

It should be noted that, the velocity reduction calculated here is only for pure current velocities. The water particles move in circles in waves with radius equal to the wave amplitude at the free surface. This radius decays quickly with water depth. According to the linear theory and for a wave period of 5 s, the wave particle motions at -20 m will decay to approximately 4% as those near the free surface. Thus, the reduction of wave particle velocities is considered secondary compared to the current reduction. Moreover,

the shielding effects from the floater on the nets are not included in the model. Because the cages are located below the floater (as shown in Figure 2), these effects are expected to be minor.

Iterative routine for calculation of static equilibrium

Because the current reduction depends on the relative angle between the vessel heading and currents, α, an iterative routine is proposed below to find the static equilibrium of the vessel-shaped fish farm under any combined wave and current condition.

1. Assume the initial value $\alpha_0 = 0$, so the current reduction can use the one shown in Figure 5(a).
2. Run static analysis of the coupled numerical model under a given wave and current condition. New equilibrium can be found and a new misalignment angle α_k is obtained.
3. Update the current reduction factor on each net panel of each fish cage based on α_k and the proposed method shown in Figure 5(b).
4. Repeat the previous two steps and obtain a new α_{k+1}. The iteration continues until the difference between α_k and α_{k+1} is within the tolerance (10^{-1} degrees).

INTEGRATED METHOD USING METAMODELS

Integrated method

This study aims to predict the misalignment angle between the vessel and the currents for any site condition. To provide an accurate estimation for a specific site, long-term environmental description with wave and current hindcast or measurement data over many years should be used. However, to perform numerical simulations for all conditions over many years will require significant computational time, and will not be feasible. Thus, approximation techniques can be applied to minimize the computational expenses. The basic approach is to approximate the computationally expensive simulation codes with surrogate models, which can be sufficiently accurate to replace the original code. The surrogate models are often called metamodels. Metamodels are popular engineering tools to minimize the computational costs and have been applied in many fields, such as design optimization and reliability assessment [22, 23, 24].

In this paper, an integrated method is proposed using metamodels for the prediction of the misalignment angle between the vessel and the currents for any site condition. The integrated method is shown in Figure 6. First, the main environmental variables with their lower and upper bounds need to be selected based on

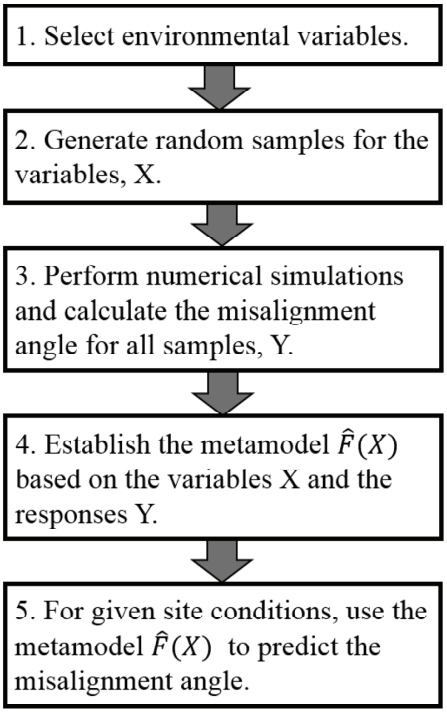

Figure 6: Flowchart for the integrated method using metamodels.

design considerations (Step 1). Initial samples of the chosen environmental variables, X, over the entire design space is required (Step 2). The initial samples provides the input for the numerical simulations, which predict the misalignment angle, Y using the iterative routine (Step 3). A metamodel, $\widetilde{F}(X)$, is then established for the misalignment angle based on X and Y. The metamodel constructs the relationship between the design variables and corresponding responses to replace the original complex numerical models (Step 4). Finally, for a given site with available environmental conditions, the misalignment angle for this specific site can be predicted efficiently using the metamodel, $\widetilde{F}(X)$ (Step 5). The methodology and discussions on the main steps involved in the integrated method is detailed as follows.

Sampling of environmental variables

The responses of the fish farm structures depend on the site condition, which normally includes wind, waves and currents. In this study, we focus on the waves and currents, and the variables include significant wave height (H_s), wave spectral peak period, T_p, mean current velocity, U_c, and the directional difference between the waves and current, $\Delta\theta$. Because the single-point mooring system makes the whole structure weathervane, the direction difference $\Delta\theta$ will determine the equilibrium heading for the structure instead of the individual wave and current directions. The variables and the corresponding lower and upper bounds are listed in Table 2.

Table 2: Design variables and their lower and upper bounds

Variables	Lower and upper bounds
H_s	0 - 8 (m)
T_p	2 - 20 (s)
U_c	0 - 1.5 (m/s)
$\Delta\theta$	0 - 180 (deg)

An initial sampling of variables over the entire design space is required, and it is a problem in the design of experiments (DOE) [25]. This problem has been studied extensively on the design and analysis of computer experiments. The commonly used DOE includes uniform design, random sampling, Latin hypercube sampling and orthogonal arrays [22]. In the case study, we employ the Latin hypercube sampling (LHS) method. LHS is a strategy for generating random sample points ensuring that all portions of the vector space is represented [26]. The LHS strategy divides the interval of each dimension into non-overlapping intervals having equal probability. Random samples in each interval of each dimension are generated and the points from each dimension are paired randomly.

In the present study, LHS method is applied for the sampling of the four environmental variables in Table 2, and 6000 pairs of samples are used as input for the numerical simulations for Step 3 in the integrated method (Figure 6).

Application of metamodels

In the integrated method, metamodels are constructed between the environmental variables and the simulated misalignment angles. With a metamodel, the misalignment angle distribution for a given site with a large database of metocean data can be predicted efficiently. There are different types of metamodels, such as Kriging models [27], neural networks [28], radial basis functions [29] and polynomial functions [30]. Detailed metamodeling strategies can refer to the above cited literature. In the current study, the Kriging model is applied.

The Kriging model estimates the value of the output from the sum of the weighted values of the known surrounding sample points, $X = (x_1, \ldots, x_n)$. The corresponding responses, $Y = (y_1, \ldots, y_n)$, of these sample points x_i are obtained from the complex numerical model simulations. Then, a predicted value $\widehat{F}(x)$ is expressed in two parts as:

$$\widehat{F}(x) = f(x) + \delta(x) \tag{8}$$

where $f(x)$ is the regression function, and $\delta(x)$ is a random function (stochastic process) to describe the

residuals. The regression functions capture the data, and the stochastic process interpolates the residuals. The regression function is a linear combination of the chosen functions, such as multivariate polynomial functions. The random process, $\delta(x)$, is assumed to have zero mean and covariance between $\delta(x_i)$ and $\delta(x_j)$:

$$Cov[\delta(x_i), \delta(x_j)] = \sigma^2 R(\theta, x_i, x_j) \tag{9}$$

where σ^2 is the process variance and $R(\theta, x_i, x_j)$ is the correlation model with parameter θ. The two common types of the correlation model are the Gaussian and exponential correlation functions. By minimizing the errors between the predictor and the data points, the parameters involved in the correlation function can be obtained.

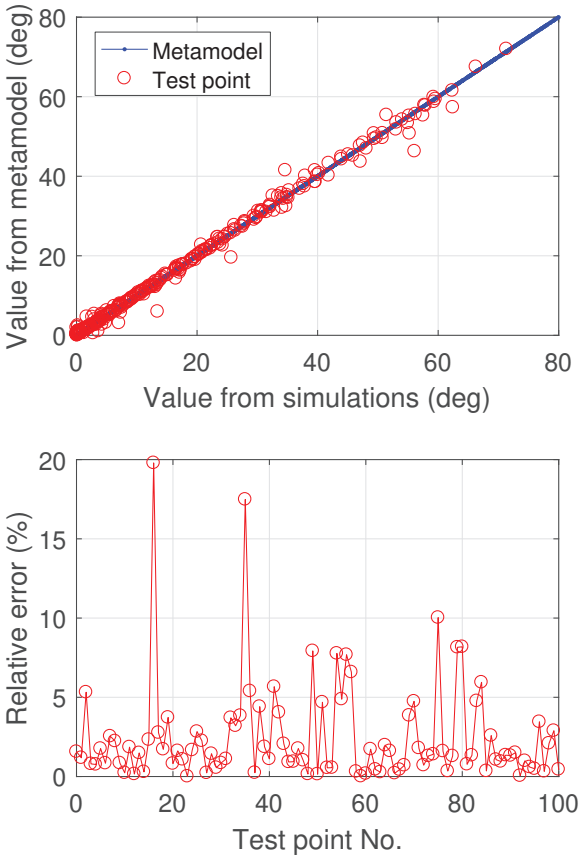

Figure 7: Validation of the Kriging metamodel using additional simulation points.

Metamodels must be validated before being used as a 'surrogate' of the numerical models. Both cross validation using available data points or validation by employing new test points can be used. Figure 7 presents the validation of the Kriging model for the calculated misalignment angle. In addition to the initial samples, 150 new samples are used for the validation. Reasonable agreements between the predicted values from Kriging model and the actual simulation results are reached. The relative errors between the

two values are also presented for the test points with misalignment angle larger than 10 degrees to avoid large errors when the values are close to 0. The relative error is defined in Eq. (10).

$$R = \left| \frac{y_i - \widetilde{y_i}}{y_i} \right| \times 100\% \tag{10}$$

where $\widetilde{y_i}$ is the predicted value using Kriging model and y_i is the actual value from numerical simulations. It is seen that except two test points, most of the relative errors are below 10%. The validation shows the acceptable accuracy of the Kriging model, and thus using this metamodel to replace the numerical simulation code is feasible. To increase the accuracy of the metamodel, more samples for simulations may be required. Furthermore, different metamodels can be employed and compared to select the most suitable model.

PREDICTION OF THE MISALIGNMENT ANGLE FOR A REFERENCE SITE

A case study is presented in this section using the proposed integrated method. The established metamodel is applied to predict the misalignment angle between the vessel and the currents for a typical exposed site for fish farms. A short description of the site condition is presented first, followed by results and discussions.

Wave and current conditions at the reference site

A reference site, Breisundet, in the west coast of Norway is selected for the case study. The coordinate of the site is 62.43901°N 5.92953°E, located close to the city Ålesund and outside Sulafjord. The water depth is 345 m. The location of the reference site is shown in Figure 8, and detailed bathymetry information near this location can refer to Ref. [31]. The wave and current conditions were measured using wave buoys and acoustic Doppler current profiler. The wave and current data for every 10 min over the period from October 2016 to November 2017 are used in the analysis. Wave spectral parameters H_s and T_p were extracted from the measurements. The current velocity was measured over the depth from the free surface to 100 m below, and the velocity at 30 m below the free surface is used for the calculation of current forces on the whole fish farm structure.

The maximum H_s is found to be 6.9 m and the maximum current velocity U_c is 1.4 m/s. Based on the

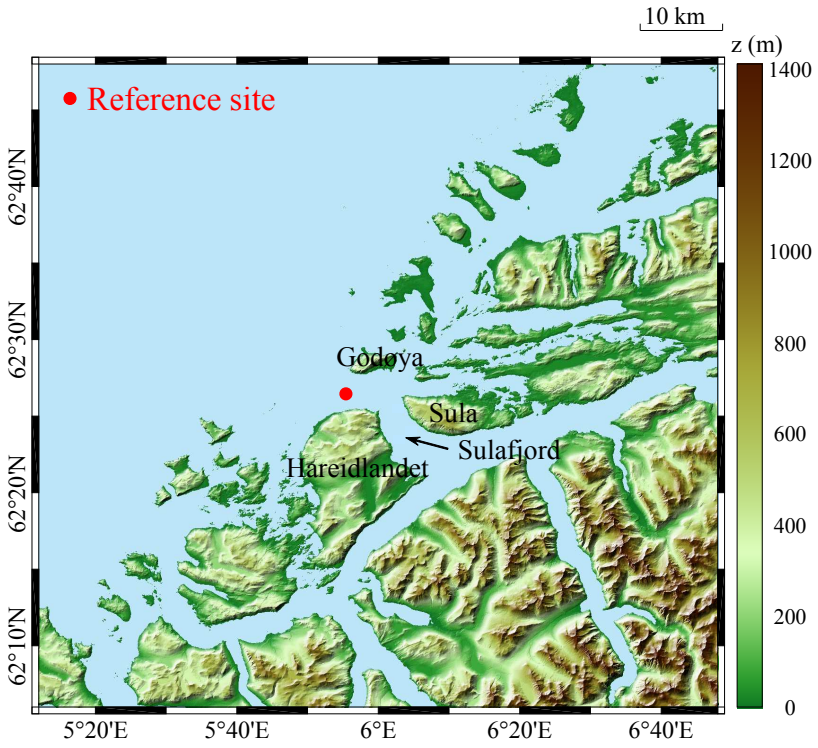

Figure 8: Map of the reference site area.

classification of the wave and current conditions in the Norsk Standard NS 9415, the maximum current condition for this site is considered as 'high exposure' ($1m/s < U_c < 1.5m/s$), while the extreme wave condition belongs to the highest wave class 'extreme exposure' ($H_s > 3m$).

Figure 9 presents the wave and the current roses for the reference site based on the one-year data. The directions are defined as the coming direction of the waves or currents. Most of the waves come from the north-west with little directional scatter. The general circulation in the local area includes tides with a period of around 12 hours and wind-driven currents. The main direction of the wind-driven currents are aligned with the main wave direction, but with more spreading compared to the waves. The tides also contribute to the currents from the east and south-east. In general, for the reference site, large waves and currents are mostly aligned or with small directional differences. Misalignment conditions with directional differences larger than 30 degrees often appear when the current velocities are less than 0.6 m/s.

In the static analysis, unidirectional irregular waves are modeled using the JONSWAP spectrum [19], where the spectral shape parameters are adjusted for different sea states. Uniform current profile is assumed for load calculation of the net panels.

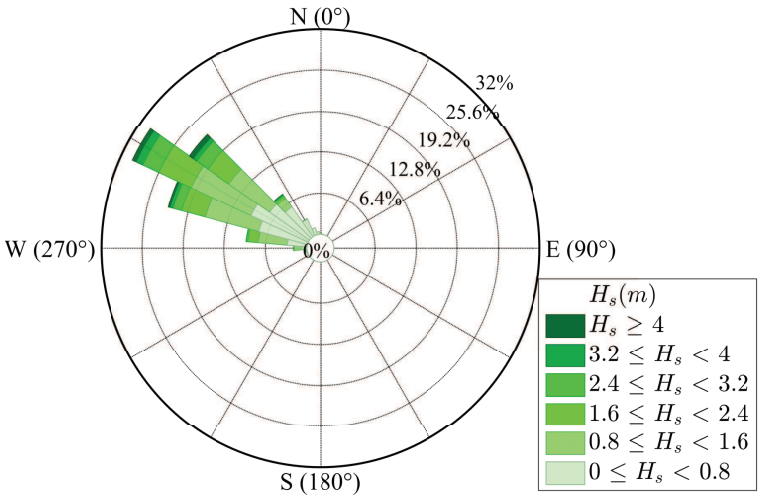

(a) Wave rose

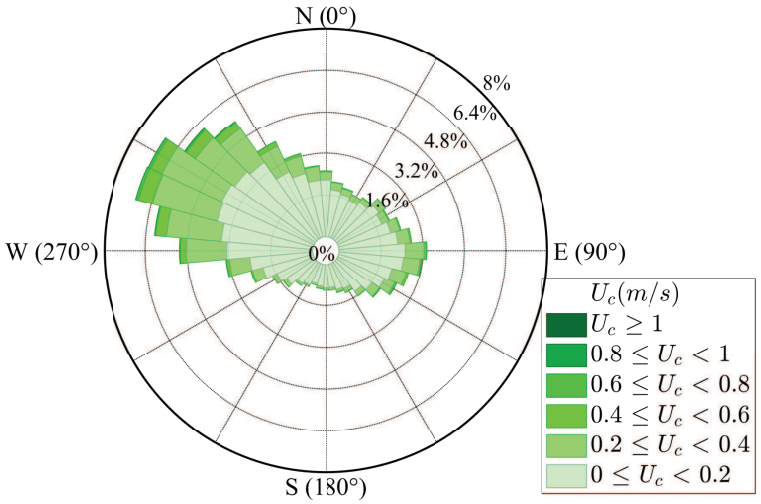

(b) Current rose

Figure 9: Wave and current roses for the reference site ('N', 'S', 'W' and 'E' refer to North, South, West and East, respectively.).

Dynamic responses

Figure 10 shows the top and side views of the static equilibrium of the fish farm structure under a typical misaligned wave and current condition in the SIMA program. It is obvious that deformation of the flexible cages is significant under the current velocity of 1.28 m/s. The individual cage deformation weakens from cage 1 to cage 5 because of the reduction in current velocity. For the same reason, deformations of the upstream net panels are observed to be larger than those of the downstream net panels within one cage. The misalignment angle between the vessel heading and the current is 22.2 degrees for the illustrated case.

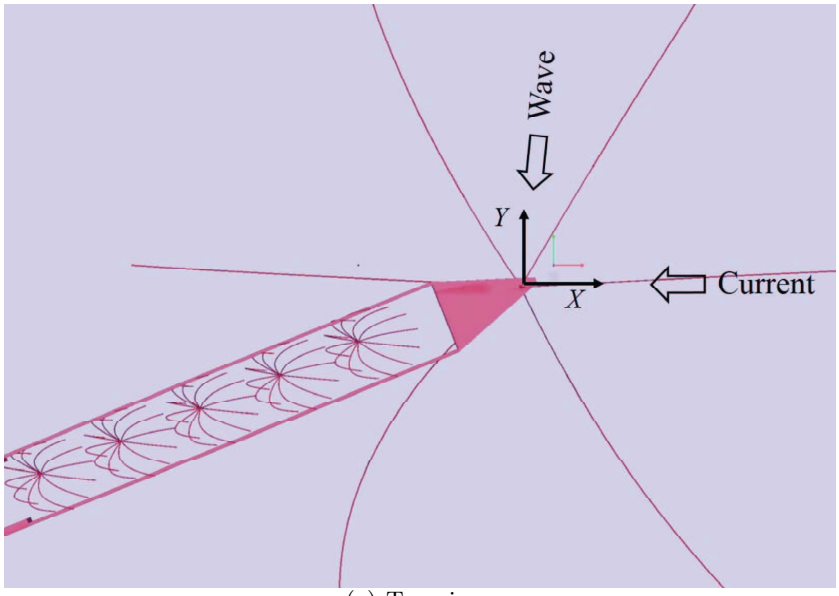

(a) Top view

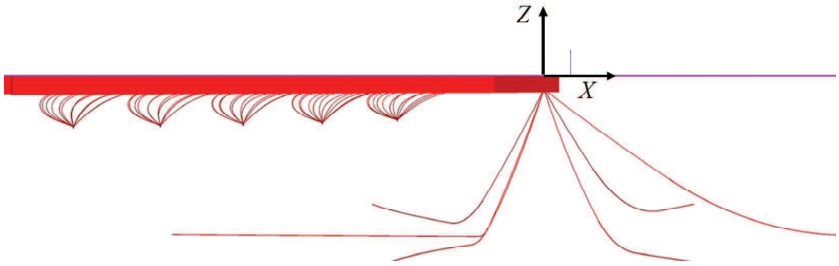

(b) Side view

Figure 10: Equilibrium condition of the fish farm structure (net solidity ratio of $S_n = 0.2$) under uniform currents (U_c=1.28 m/s, Dir_c = 180 deg) and waves (H_s =6.29 m, T_p = 10.21 s, Dir_w = 261 deg).

Misalignment angle

By using the one-year combined wave and current conditions and the established metamodel, the misalignment angle between the vessel and the currents are predicted for the reference site. Figure 11 presents the probability distribution of occurrence and probability of exceedance for the misalignment angle over the studied period. The results are compared for S_n of 0.2 and 0.3 for the nets.

For both cases, it is seen that the vessel and the currents are almost aligned for 40% of the situations with misalignment angle less than 5 degrees. The total probability of occurrence with the misalignment angle over 20 degrees is around 20% for this site. Except for around 3% higher probability for almost aligned condition with S_n of 0.3, the misalignment angle distributions are almost the same using two different S_n.

Intuitively, the rapid increase of the drag coefficient C_D with S_n will result in much larger drag forces on a fixed net panel. However, larger S_n causes more severe net cage deformation and current reduction

in the downstream cages. These factors will prevent the rapid increase of the total drag forces on the five cages. In addition, the final misalignment angle of the whole structure corresponds to an equilibrium state due to the wave and current forces acting on the floater and the cages. The forces on the floater are found to contribute more than those on the cages for the two studied S_n, especially when the misalignment angle exceeds 10 degrees. Thus, the sensitivity study shows minor influences from S_n on the distribution of the misalignment angle. It should be mentioned that the influence of the global flow field due to high S_n of the nets is not addressed in the simulation. When S_n is higher, the global flow field can be disturbed and the misalignment angle may be affected.

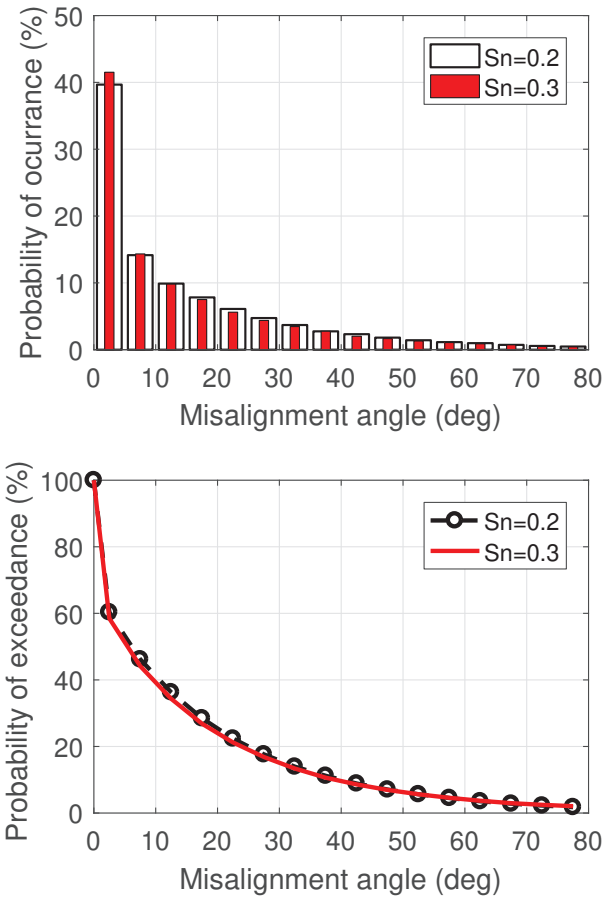

Figure 11: Probability of occurrence and exceedance for the misalignment angle during one year.

Reduced current velocity in the cage

The current reduction due to shielding effects from upstream net panels plays an important role when assessing the flow conditions in the cage. Several experimental studies on the current reduction in the fish cages can be found in the literature [11, 32]. These studies reported up to 20% of flow reduction after a single net panel with various solidity ratios. A few field measurements have reported more than 30%

Table 3: Average current reduction factors, R, inside each cage under different misalignment angle α.

	Sn=0.2					Sn=0.3				
α	Cage 1	Cage 2	Cage 3	Cage 4	Cage 5	Cage 1	Cage 2	Cage 3	Cage 4	Cage 5
0 °	0.106	0.285	0.429	0.544	0.635	0.195	0.478	0.661	0.780	0.858
5°	0.106	0.225	0.303	0.345	0.365	0.195	0.389	0.502	0.559	0.585
10°	0.106	0.201	0.240	0.225	0.225	0.195	0.352	0.411	0.389	0.389
15°	0.106	0.181	0.186	0.186	0.186	0.195	0.320	0.328	0.328	0.328
20°	0.106	0.175	0.175	0.175	0.175	0.195	0.311	0.311	0.286	0.311
25°	0.106	0.149	0.149	0.149	0.149	0.195	0.269	0.269	0.269	0.269
30°	0.106	0.144	0.144	0.144	0.144	0.195	0.260	0.260	0.260	0.260
35°	0.106	0.139	0.139	0.139	0.139	0.195	0.251	0.251	0.251	0.251
40°	0.106	0.133	0.133	0.133	0.133	0.195	0.242	0.242	0.242	0.242

of current reduction in a single cage with solidity ratio around 0.15 [33]. Table 3 presents the average reduction factor for S_n of 0.2 and 0.3. The numbers are calculated by taking the mean value of the reduction factors from the net panels located in the upstream of the cage. The calculations are based on Eqs. (5) to (7) and the method shown in Figure 5, and the estimation is based on non-deformed net panels.

It can be observed from Table 3 that the current reduction factor increases substantially from Cage 1 to Cage 5 when S_n rises and the misalignment angle (α) is below 10 degrees. Such an increase is due to the wake shielding effects as the net panels in the following cages are positioned behind the upstream panels. The average reduction factor in Cage 5 when the vessel is aligned with the currents is over 60% with S_n of 0.2, and over 80% with S_n of 0.3. This means when the incoming current velocity is 1 m/s, the average current velocity inside Cage 5 is lower than 0.4 m/s and 0.2 m/s, respectively. The high reduction factor indicates lower levels of dissolved oxygen and increased wastes from the upstream cages. Both factors may significantly affect the fish health [34]. With a misalignment angle larger than 15 degrees, the current reduction factors reach similar values for Cage 2 to Cage 5. In this case, the current direction is oblique relative to the vessel heading, and many net panels in Cages 2 to 5 are exposed to the current and not sheltered by other net panels. Thus, the current reduction factor is lower. S_n has a significant influence on the current reduction factor. When S_n increases from 0.2 to 0.3, the current reductions at different cages and misalignment angles increase by over 75% on average.

The flow condition inside the cages directly influences fish health and should be used as a criterion to assess whether the DP system is required. However, to quantify the flow condition inside each cage is a challenging task. The flow is affected by many factors, including the current reduction between the cages, the solidity ratio of the nets, the vessel motions, the deformation of the cages, and fish movements. Among

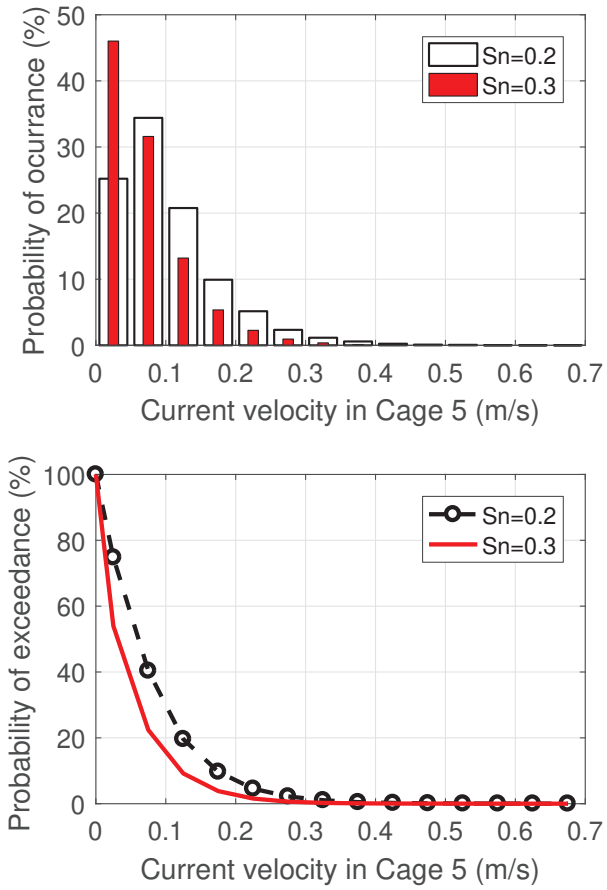

Figure 12: Probability of occurrence and exceedance for the current velocity in Cage 5 during one year.

these factors, it is obvious that current reduction between the cages depends greatly on the misalignment angle between the structure and currents, which is related to the operation of DP system. Thus, in this case study, we only focus on predicting the current velocity in the cages considering the reduction factors.

Based on the estimated reduction factors from Table 3 for different misalignment angles and the one-year current velocities at the reference site, distribution of the current velocities inside each cage can be obtained. Because Cage 5 will experience the worst flow conditions among the five cages, the flow condition inside Cage 5 is emphasized. Figure 12 presents the probability of occurrence and exceedance for the current velocity inside Cage 5 during one-year period. It is obvious that S_n significantly affects the current velocity. The probability of having current velocity less than 0.1 m/s is over 80% with S_n of 0.3, and is around 70% with S_n of 0.2.

To provide a better overview between the current velocity in the cage and the usage of DP system, a reference value for the current velocity is needed. Some studies have reported that the current velocity and dissolved oxygen saturation are correlated [35]. The dissolved oxygen saturation is considered a critical parameter affecting the fish growth and performance. Ref. [35] has reported 30% to 90% of

oxygen saturation with the current velocity between 0.05 m/s to 0.25 m/s. It was also found that 53% of saturation were deemed physiologically suitable for maximum growth of the fish [36]. As many other factors (e.g., temperature and fish movements) also influence the oxygen saturation inside the fish cage, it is difficult to provide a reference value for the current velocity. However, for further discussions in this study, we assume three reference values for the current velocity, 0.05 m/s, 0.08 m/s and 0.1 m/s, respectively. Once the current velocity in Cage 5 is below these reference values, DP systems will be activated to rotate the vessel and to improve the flow condition.

The probability of using DP systems for the three reference current velocities are presented in Table 4. More than 40% of the time the DP system is required for all the studies cases. The increase of S_n value brings significant rise on the DP usage. This suggests the biofouling on the nets need to be prevented to avoid the increase of S_n. It is also noted that usage of DP systems depends greatly on the selection of the reference current velocity inside the cage. If the reference value is 0.1 m/s, the probability for using DP systems is over 70% for this site. It should be mentioned that the probabilities obtained here is based on the assumption that the current velocity is only affected by the shielding effects from upstream cages. Influences from other factors need to be considered in the future work.

Table 4: Probability of using DP systems for three reference current velocities.

Reference current velocity	0.05 m/s	0.08 m/s	0.1 m/s
Probability ($S_n = 0.2$)	42.4 %	66.3%	70.0%
Probability ($S_n = 0.3$)	61.8 %	81.3%	84.2%

CONCLUSIONS AND FUTURE WORK

This paper presents a numerical study to predict the misalignment angle between the heading of the vessel-shaped offshore fish farm and the incoming currents. The misalignment angle is useful in estimation of the flow conditions in the cages so as to facilitate the design of the dynamic positioning system for the fish farm. An integrated method using metamodels is proposed. The metamodels are used as surrogates for the complex numerical simulations. The probability distribution of the misalignment angle for a reference site in Norway has been predicted. It was shown that the vessel and the currents are aligned for 40% of the time during the one-year period for the reference site using two solidity ratios of 0.2 and 0.3 for the nets. By estimating the averaged current reduction factors inside each cage under various misalignment angles, the distribution of the current velocity is obtained. By assuming three values for

the reference current velocity as criteria, the probability of requiring DP system is predicted. It is found the solidity ratio and the reference current velocity have significant influences on the estimation of DP requirement. The metamodel used in this work proves to be efficient for estimation of the responses under a large number of environmental conditions, and it can be used for similar applications.

In this study, the misalignment angle is based on static calculations where the whole coupled system reach a equilibrium under mean wave drift forces on the vessel and mean current forces on the mooring lines and the fish nets. However, in real-life situations, the whole system experiences dynamic motions under irregular waves and currents. The mean position in dynamic conditions may deviate from the one calculated from static conditions due to additional mean forces from waves on the fish nets. Moreover, the wind forces on the super structures may also influence the misalignment angle. These aspects need to be studied in the future work.

Furthermore, the flow conditions inside the fish cages are important for the fish health, and quantitative methods to predict the flow conditions are essential. It is recommended to study the flow conditions inside the fish cages using more advanced numerical (e.g., computational fluid dynamics) or experimental methods considering the deformation of the nets and the interactions between the cages. The quantitative analysis of the flow condition can provide a better criteria to improve the design of the DP system. Additionally, the upper limits of the current velocity are also relevant to the fish health and welfare. This aspect should be taken into consideration in future studies when designing the DP system and the whole fish farm structure.

ACKNOWLEDGEMENTS

The measurement data of the reference site are acquired for Norwegian Public Roads Administration (NPRA) and made available online by the Norwegian Meteorological Institute. The authors acknowledge Dr. Birgitte R. Furevik from the Norwegian Meteorological Institute and Dr. Jon Albretsen from the Institute of Marine Research in Norway for valuable discussions on the data.

References

[1] Burnell, G., and Geoff, A, eds, 2009. *New technologies in aquaculture: Improving production efficiency, quality and environmental management.* Cambridge, UK, Elsevier, pp. 895–913.

[2] SalMar Group, 2016. Offshore fish farming - a new era in fish farming is on its way. Available at http://www.salmar.no/en/offshore-fish-farming-a-new-era. Accessed: 2017-10-07.

[3] Berge, A., 2017. Today, 'Ocean Farm 1' comes to Froya. Available at http://salmonbusiness.com/today-ocean-farm-1-comes-to-froya/. Accessed: 2017-10-20.

[4] Li, L., and Ong, M. C., 2017. "A preliminary study of a rigid semi-submersible fish farm for open seas". In Proceedings of the 36th International Conference on Ocean, Offshore and Arctic Engineering, June 25-30, 2017, Trondheim, Norway.

[5] reference5, 2017. Havfarm. Available at http://www.nordlaks.no/Havfarmene. Accessed: 2018-02-10.

[6] Li, L., Jiang, Z., and Ong, M. C., 2017. "A preliminary study of a vessel-shaped offshore fish farm concept". In Proceedings of the 36th International Conference on Ocean, Offshore and Arctic Engineering, June 25-30, 2017, Trondheim, Norway.

[7] Li, L., Jiang, Z., Høiland, A. V., and Ong, M. C., 2018. "Numerical analysis of a vessel-shaped offshore fish farm". *Journal of Offshore Mechanics and Arctic Engineering,* ***140***(4), p. 041201.

[8] Klebert, P., Lader, P., Gansel, L., and Oppedal, F., 2013. "Hydrodynamic interactions on net panel and aquaculture fish cages: A review". *Ocean Engineering,* ***58***, pp. 260–274.

[9] Klebert, P., Patursson, Ø., Endresen, P. C., Rundtop, P., Birkevold, J., and Rasmussen, H. W., 2015. "Three-dimensional deformation of a large circular flexible sea cage in high currents: Field experiment and modeling". *Ocean Engineering,* ***104***, pp. 511–520.

[10] Gansel, L. C., Rackebrandt, S., Oppedal, F., and McClimans, T. A., 2014. "Flow fields inside stocked fish cages and the near environment". *Journal of Offshore Mechanics and Arctic Engineering,* ***136***(3), p. 031201.

[11] Bi, C.-W., Zhao, Y.-P., Dong, G.-H., Xu, T.-J., and Gui, F.-K., 2013. "Experimental investigation of the reduction in flow velocity downstream from a fishing net". *Aquacultural Engineering,* ***57***, pp. 71–81.

[12] Gansel, L. C., McClimans, T. A., and Myrhaug, D., 2012. "Flow around the free bottom of fish cages in a uniform flow with and without fouling". *Journal of Offshore Mechanics and Arctic Engineering,* ***134***(1), p. 011501.

[13] Moe-Føre, H., Lader, P., Lien, E., and Hopperstad, O., 2016. "Structural response of high solidity net cage models in uniform flow". *Journal of Fluids and Structures,* ***65***, pp. 180–195.

[14] MARINTEK, 2015. *SIMO - Theory Manual Version 4.6.* MARINTEK, Trondheim, Norway, pp. 6–126.

[15] MARINTEK, 2015. *RIFLEX Theory Manual Version 4.6.* MARINTEK, Trondheim, Norway, pp. 3–107.

[16] MARINTEK, 2016. *Modelling of Aquacuture Net Cages in SIMA.* MARINTEK, Trondheim, Norway, pp. 4–21.

[17] DNV, 2008. *Wadam theory manual.* Det Norske Veritas, Oslo, Norway, pp. 7–79.

[18] Tian, X., Ong, M. C., Yang, J., and Myrhaug, D., 2014. "Large-eddy simulation of the flow normal to a flat plate including corner effects at a high Reynolds number". *Journal of Fluids and Structures,* ***49***, pp. 149–169.

[19] DNV, 2010. *Recommended Practice DNV-RP-C205, Environmental conditions and enviromental loads.* Det Norske Veritas, Oslo, Norway, pp. 24–122.

[20] Løland, G., 1993. "Current forces on, and water flow through and around, floating fish farms". *Aquaculture International,* ***1***(1), pp. 72–89.

[21] Lader, P. F., and Enerhaug, B., 2005. "Experimental investigation of forces and geometry of a net cage in uniform flow". *IEEE Journal of Oceanic Engineering,* ***30***(1), pp. 79–84.

[22] Wang, G. G., and Shan, S., 2007. "Review of metamodeling techniques in support of engineering design optimization". *Journal of Mechanical Design,* ***129***(4), pp. 370–380.

[23] Jiang, Z., and Gu, M., 2010. "Optimization of a fender structure for the crashworthiness design". *Materials & Design,* ***31***(3), pp. 1085–1095.

[24] Li, L., Jiang, Z., and Ong, M. C., 2018. "Design optimization of mooring system: an application to a vessel-shaped offshore fish farm". *Engineering Structures.* Under review.

[25] Simpson, T. W., Lin, D. K., and Chen, W., 2001. "Sampling strategies for computer experiments: design and analysis". *International Journal of Reliability and Applications,* ***2***(3), pp. 209–240.

[26] McKay, M. D., Beckman, R. J., and Conover, W. J., 2000. "A comparison of three methods for selecting values of input variables in the analysis of output from a computer code". *Technometrics,* ***42***(1), pp. 55–61.

[27] Cressie, N., 1988. "Spatial prediction and ordinary Kriging". *Mathematical Geology,* ***20***(4), pp. 405–421.

[28] Papadrakakis, M., Lagaros, N. D., and Tsompanakis, Y., 1998. "Structural optimization using evolution strategies and neural networks". *Computer Methods in Applied Mechanics and Engineering,* ***156***(1-4), pp. 309–333.

[29] Dyn, N., Levin, D., and Rippa, S., 1986. "Numerical procedures for surface fitting of scattered data by radial functions". *SIAM Journal on Scientific and Statistical Computing,* ***7***(2), pp. 639–659.

[30] De Boor, C., and Ron, A., 1990. "On multivariate polynomial interpolation". *Constructive Approximation,* ***6***(3), pp. 287–302.

[31] Wang, J., Li, L., Jakobsen, J. B., and Haver, S. K., 2019. "Metocean conditions in a norwegian fjord in relation to the floating bridge design". *Journal of Offshore Mechanics and Arctic Engineering,* ***141***(2), p. 021604.

[32] Turner, A. A., Jeans, T. L., and Reid, G. K., 2016. "Experimental investigation of fish farm hydrodynamics on 1:15 scale model square aquaculture cages". *Journal of Offshore Mechanics and Arctic Engineering,* ***138***(6), p. 061201.

[33] DeCew, J., Fredriksson, D., Lader, P., Chambers, M., Howell, W., Osienki, M., Celikkol, B., Frank, K., and Høy, E., 2013. "Field measurements of cage deformation using acoustic sensors". *Aquacultural Engineering,* ***57***, pp. 114–125.

[34] Johansson, D., Juell, J.-E., Oppedal, F., Stiansen, J.-E., and Ruohonen, K., 2007. "The influence of the pycnocline and cage resistance on current flow, oxygen flux and swimming behaviour of Atlantic salmon (Salmo salar L.) in production cages". *Aquaculture,* ***265***(1), pp. 271–287.

[35] Solstorm, D., Oldham, T., Solstorm, F., Klebert, P., Stien, L. H., Vågseth, T., and Oppedal, F., 2018. "Dissolved oxygen variability in a commercial sea-cage exposes farmed Atlantic salmon to growth limiting conditions". *Aquaculture,* ***486***, pp. 122–129.

[36] Remen, M., Sievers, M., Torgersen, T., and Oppedal, F., 2016. "The oxygen threshold for maximal feed intake of Atlantic salmon post-smolts is highly temperature-dependent". *Aquaculture,* ***464***, pp. 582–592.